Shape coexistence in neutron-deficient Hg isotopes studied via lifetime measurements in ^{184,186}Hg and two-state mixing calculations

L. P. Gaffney,[1,2,*] M. Hackstein,[3,†] R. D. Page,[1,‡] T. Grahn,[1,4] M. Scheck,[1,5] P. A. Butler,[1] P. F. Bertone,[6]
N. Bree,[2] R. J. Carroll,[1] M. P. Carpenter,[6] C. J. Chiara,[6,7] A. Dewald,[3] F. Filmer,[1] C. Fransen,[3]
M. Huyse,[2] R. V. F. Janssens,[6] D. T. Joss,[1] R. Julin,[4] F. G. Kondev,[8] P. Nieminen,[4] J. Pakarinen,[1,4,9]
S. V. Rigby,[1] W. Rother,[3] P. Van Duppen,[2] H. V. Watkins,[1] K. Wrzosek-Lipska,[2] and S. Zhu[6]

[1]*Oliver Lodge Laboratory, University of Liverpool, Liverpool L69 7ZE, United Kingdom*
[2]*KU Leuven, Instituut voor Kern- en Stralingsfysica, B-3001 Leuven, Belgium*
[3]*Institut für Kernphysik, Universität zu Köln, Zülpicher Strasse 77, D-50937 Köln, Germany*
[4]*Department of Physics, University of Jyväskylä, Post Office Box 35, FI-40014 Jyväskylä, Finland*
[5]*Institut für Kernphysik, TU Darmstadt, D-64289 Darmstadt, Germany*
[6]*Physics Division, Argonne National Laboratory, Argonne, Illinois 60439, USA*
[7]*Department of Chemistry and Biochemistry, University of Maryland, College Park, Maryland 20742, USA*
[8]*Nuclear Engineering Division, Argonne National Laboratory, Argonne, Illinois 60439, USA*
[9]*CERN-ISOLDE, CERN, CH-1211 Geneva 23, Switzerland*

The neutron-deficient mercury isotopes, ^{184,186}Hg, were studied with the recoil distance Doppler-shift method using the Gammasphere array and the Köln plunger device. The differential decay curve method was employed to determine the lifetimes of the yrast states in ^{184,186}Hg. An improvement on previously measured values of yrast states up to 8^+ is presented as well as first values for the 9_3 state in ^{184}Hg and 10^+ state in ^{186}Hg. $B(E2)$ values are calculated and compared to a two-state mixing model which utilizes the variable moment of inertia model, allowing for extraction of spin-dependent mixing strengths and amplitudes.

I. INTRODUCTION

Nuclei exhibiting different shapes at low energy have been of interest in nuclear structure ever since the discovery of a large jump in the mean-squared charge radius, associated with a dramatic change in shape between ^{187}Hg and ^{185}Hg observed in isotope shift measurements [1]. Calculations based on Strutinsky's shell-correction method [2] interpreted this result as a transition from a weakly deformed oblate to a more pronounced prolate-deformed shape. Further isotope shift measurements reveal that the weakly deformed oblate character extends down to $A = 182$ in the even-mass Hg isotopes [3]. Calculations in these isotopes using the Nilsson-Strutinsky approach [4] predict two deformed minima, where the lowest-energy minimum corresponds to an oblate shape, $\beta \simeq -0.15$, and the second to a more deformed prolate shape with $\beta \simeq 0.27$. In shell-model terms, these minima are associated with a proton zero-particle-two-hole configuration, $\pi(0p\text{-}2h)$, and a two-proton excitation across the $Z = 82$ shell gap yielding a $\pi(2p\text{-}4h)$ configuration, respectively.

Spectroscopy of the even-mass mercury isotopes reveals a systematic trend of the intruding 0_2^+ bandhead (shown in Fig. 1) which minimizes in energy near the neutron midshell at $N = 104$. The excited states built upon these configurations become yrast above $I^\pi = 4^+$ for $A \leqslant 186$, and the 2^+ levels become close enough in energy to mix strongly.

Large $E0$ components in $2_2^+ \rightarrow 2_1^+$ transitions indicate a large degree of mixing. An attempt to understand the mixing between the bands was made by measuring this $E0$ component in-beam in ^{180}Hg [8] and ^{186}Hg [9]. The conversion coefficient of this transition can also be measured following β decay, and there is an effort to provide more experimental data in this region [10]. Mixing of the 0^+ states can be quantified by comparison of $\rho(E0)^2$ values [11,12] which have been experimentally determined in ^{180}Hg [13], ^{184}Hg [14], and ^{188}Hg [15]. As described in a recent review on the topic [16], the microscopic shell-model approach and the theoretical mean-field approach can both successfully reproduce the observed mixing. An analysis of α-decay hindrance factors [13,17] indicates a smaller prolate contribution to the ground-state band 0^+ state.

To determine the magnitude and type of deformation of the two bands and their mixing strength, and to test the picture of shape coexistence, more precise data are required on the absolute transition strengths between the excited states of the nuclei in this mass region. Lifetimes of excited states in ^{180,182}Hg have been recently measured by this collaboration [18,19]. To extend this knowledge and address these missing data, lifetime measurements of excited states in ^{184,186}Hg have been performed. Partial level schemes of the nuclei studied in this work are given in Fig. 2.

II. EXPERIMENTAL DETAILS

Excited states in ^{184}Hg and ^{186}Hg were populated in the heavy-ion-induced, fusion-evaporation reactions ^{148}Sm(^{40}Ar,4n)^{184}Hg and ^{150}Sm(^{40}Ar,4n)^{186}Hg, at beam

---

*Corresponding author (^{184}Hg): Liam.Gaffney@fys.kuleuven.be
†Corresponding author (^{186}Hg): hackstein@ikp.uni-koeln.de
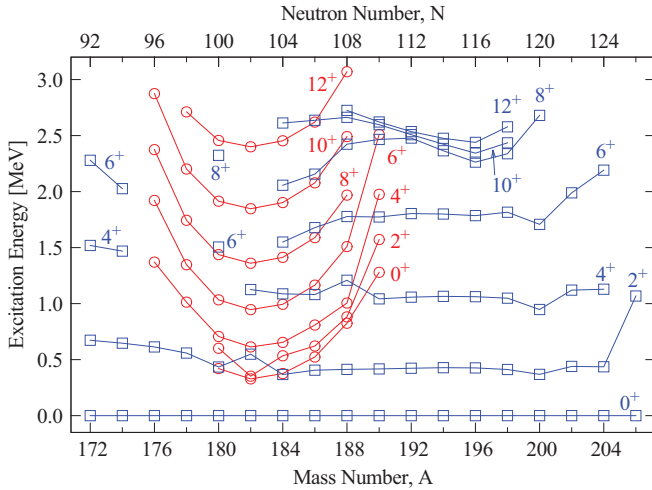‡Corresponding author (calculations): rdp@ns.ph.liv.ac.uk

FIG. 1. (Color online) Level energy systematics of even-mass mercury isotopes. Red circles refer to the assumed intruder states while blue squares refer to the assumed oblate states, guided by the results of the calculations in this work and that of Ref. [5]. The figure is an updated version of that in Ref. [6] using data taken from the National Nuclear Data Center database [7].

energies of 200 and 195 MeV. The average recoil velocity was $v/c = 1.94\%$ and 1.90%, respectively. The primary beam

was provided by the ATLAS facility at the Argonne National Laboratory and delivered to the target position inside the Gammasphere spectrometer. The latter nominally consists of 110 Compton-suppressed, high-purity Ge detectors [22] arranged into 17 rings of constant polar angle, θ, with respect to the beam. For this experiment, 100 detectors split into 16 rings were in use. The Köln plunger device was installed at the target position to allow for the recoil distance Doppler-shift (RDDS) lifetime measurements. The distance of the 11-mg/cm^2-thick Au stopper foil was varied with respect to the 0.6-mg/cm^2-thick Sm target within the range 2–2000 μm and data were taken at 12 distances for ^{184}Hg (10 for ^{186}Hg).

For the analysis of the data, $\gamma\gamma$-coincidence matrices were built using GSSORT [23] and the ROOT framework [24]. The data from different HPGe detectors of Gammasphere were grouped by rings at similar angles. In the analysis of ^{184}Hg, the lifetimes are obtained by taking the weighted average of the lifetimes for different rings. Here, it was possible to obtain the velocity independently for each ring, utilizing the measured Doppler shift of the peaks. In the case of ^{186}Hg, where measurement times were shorter, the lifetimes were derived directly from the weighted average of the intensities while the velocity was obtained by weighting the velocities from the individual $\gamma\gamma$-coincidence spectra for all combinations of ring pairs.

Typical $\gamma\gamma$-coincidence spectra obtained during the experiment are presented in Fig. 3, in which it is possible to see the variation of intensity of the fully Doppler-shifted component
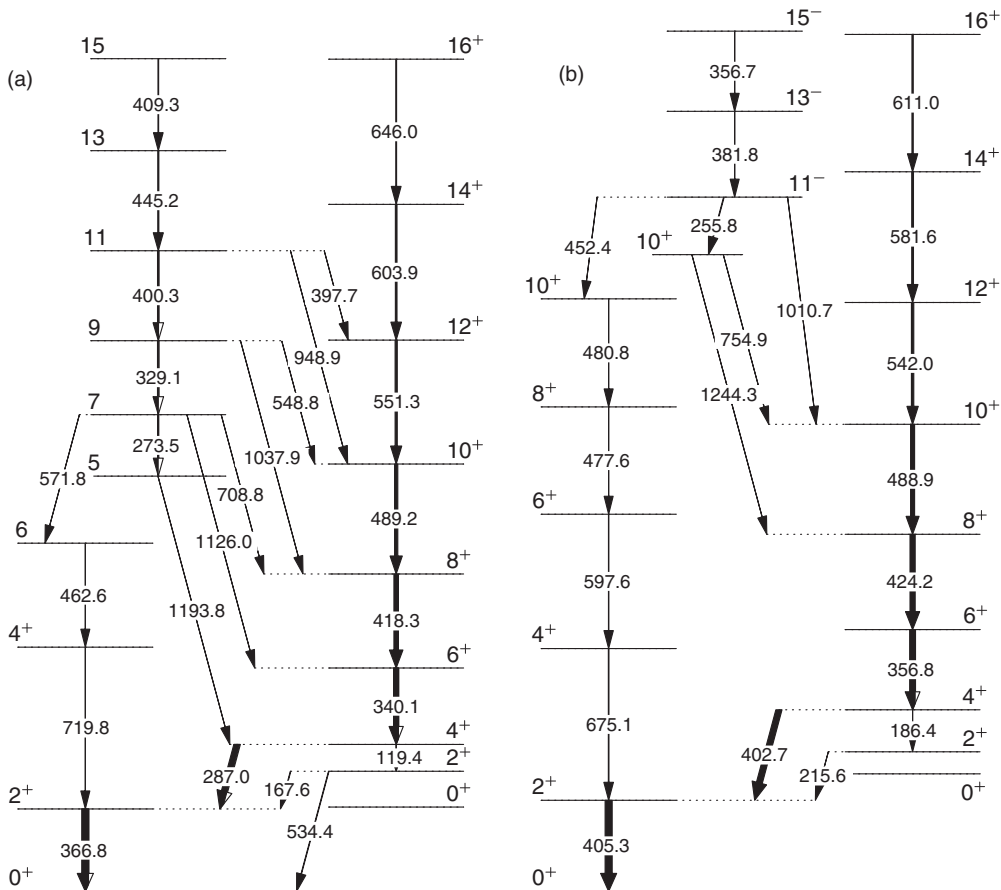

FIG. 2. Partial level schemes of (a) ^{184}Hg and (b) ^{186}Hg showing states of interest. Data are taken from Refs. [20,21].
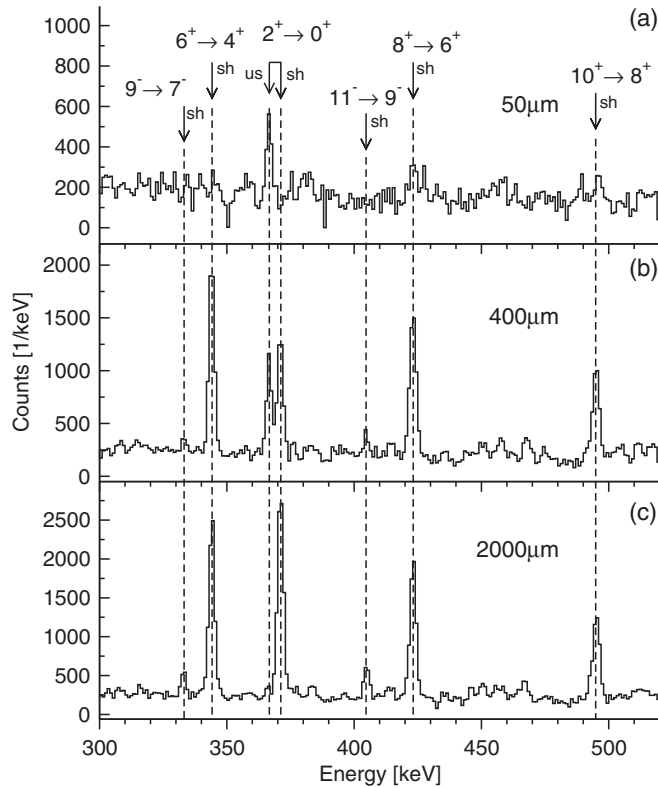
FIG. 3. γ-ray spectra from the Gammasphere detectors at $\theta \approx 53°$, gated on the shifted (sh) component of the $4_1^+ \rightarrow 2_1^+$ transition in ^{184}Hg at a target-to-stopper distance of (a) 50 μm, (b) 400 μm, and (c) 2000 μm. Transitions which feed the 4_1^+ state only have their shifted (sh) component in coincidence, while one also observes the unshifted (us) component of the $2_1^+ \rightarrow 0_1^+$ depopulating transition.

of the depopulating transition, I_{sh}, with increasing distance. At the smallest distances the flight times of the nuclei are very short, leading to few γ rays emitted in flight. Consequently, when gating in the γ-γ matrix, a low number of events are observed, an effect present in Fig. 3(a).

To account for the varying measurement time at different target-to-stopper distances, the intensities had to be normalized. For ^{184}Hg, the distances were normalized by employing a gate on the total intensity of the 340-keV $6_1^+ \rightarrow 4_1^+$ transition and averaging the intensities of the 287-keV $4_1^+ \rightarrow 2_1^+$ and 367-keV $2_1^+ \rightarrow 0_1^+$ transitions at all angles. For ^{186}Hg, all possible $\gamma\gamma$ coincidences for the yrast transitions up to the 10_1^+ state, in spectra with $\theta < 90°$, were used for the normalization. The use of the coincidence differential decay curve method (DDCM) eradicates the influence of recoil deorientation [25].

In the analysis of ^{184}Hg, lifetimes were obtained using the prescriptive coincidence DDCM [26,27]. While here we explain only the features of the method that are required for this analysis, the full details are contained in Refs. [26,27], to which the reader is referred for more information. The coincidence technique allows for the elimination of systematic errors usually introduced in RDDS-singles measurements by the unknown feeding history from states that lie higher in energy. The decay curves, as a function of distance, x, for this analysis were constructed using gates on the shifted component

of the yrast transition directly feeding the state of interest, ensuring a significant simplification whereby the lifetime is determined using only the ratio of the unshifted (I_{us}) and the time derivative of the fully shifted (I_{sh}) components of the depopulating transition:

$$\tau(x) = \frac{I_{us}(x)}{\frac{d}{dt}I_{sh}(x)}. \tag{1}$$

Typical fits of continuously connected second-order polynomials, performed with NAPATAU [28,29], are illustrated in Fig. 4. The lifetime is determined at every distance and should sit at a constant value. Deviations from this behavior indicate systematic effects, which can be identified easily with this method. The weighted average, τ_{av}, is taken of the points inside of the sensitivity region, i.e., where the derivative of the decay curve is largest.

Lifetimes of the yrast states of ^{186}Hg up to the 10_1^+ state were similarly determined with the exception of the 4_1^+ state.
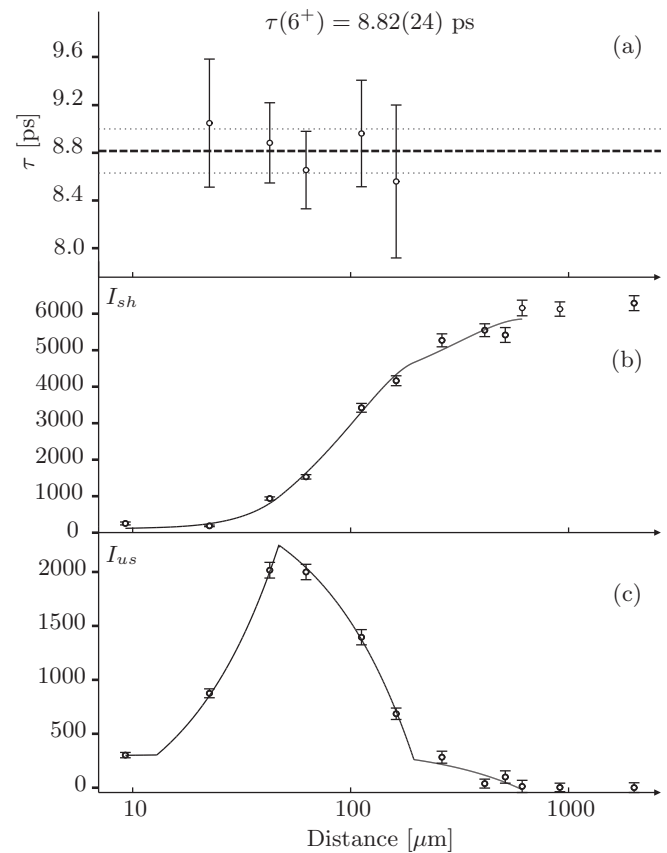

FIG. 4. (a) Lifetime values, τ, extracted at each distance in the sensitive region, for the 340-keV $6_1^+ \rightarrow 4_1^+$ transition in ^{184}Hg, measured in the detectors at $\theta \approx 53°$. The dashed and dotted lines show the weighted average and the associated uncertainty, respectively. (b) Normalized intensity curve for the shifted component, I_{sh}, fitted (solid line) with a function consisting of continuous, piecewise second-order polynomials. (c) Normalized intensity curve for the unshifted component, I_{us}. The curve in (c) is proportional to the derivative of that in (b) and both curves are fitted simultaneously. According to Eq. (1), the ratio of these gives the lifetime of the state, shown in (a).
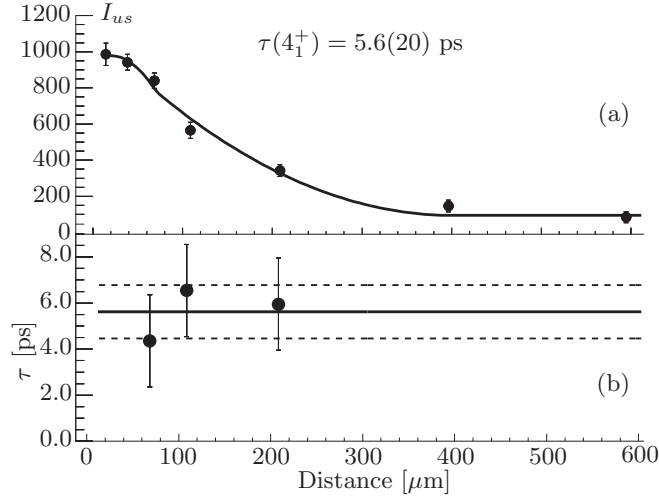
FIG. 5. (a) The normalized intensity of the unshifted component of the $4_1^+ \to 2_1^+$ depopulating transition in ^{186}Hg. The fitted line is as in Fig. 4. (b) Lifetime values extracted at each distance in the sensitive region. The solid and dashed lines show the weighted average and the associated uncertainty.
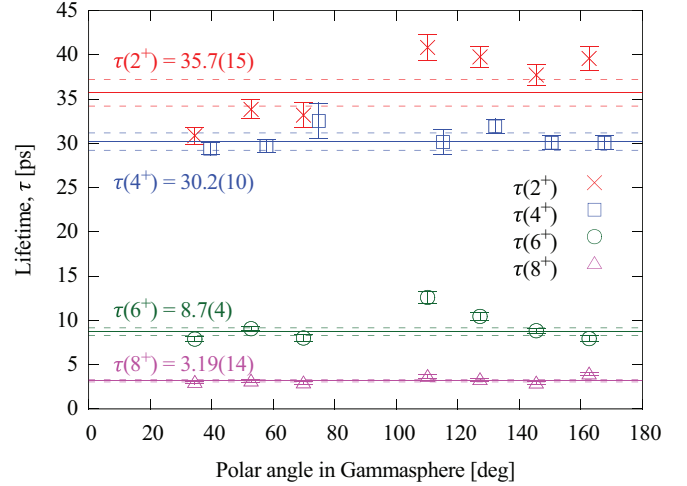

FIG. 6. (Color online) Lifetimes of yrast states in ^{184}Hg as a function of angle. The weighted average and 1σ uncertainty, calculated from the weighted standard deviation, for each state are denoted by the solid and dashed lines, respectively. Please note, the $\tau(4^+)$ values are offset by $5°$ on the x axis to maintain clarity and some individual error bars may be smaller than the marker size.

In this case, the near doublet of the $4_1^+ \to 2_1^+$ and $2_1^+ \to 0_1^+$ transitions rendered it problematic to use the simple "gate from above" method. Instead, the method of "gating from below" [30] was used. The corresponding τ plot for the 4_1^+ state is found in Fig. 5. The intensities involving the 6_1^+ and 4_1^+ analysis were corrected for a contamination from the $15_2^- \to 13_2^-$ transition, using a gate on the $13_2^- \to 11_2^-$ transition.

III. RESULTS

The final weighted averages of the mean lifetimes of all states studied are shown in Table I along with the transition strengths, $B(E2)$, and absolute transitional quadrupole moments, $|Q_t|$, of the depopulating yrast transitions. Transition quadrupole moments, Q_t, are related to the $B(E2)$ values assuming a rotating quadrupole deformed nucleus using the

rotational model:

$$B(E2; I \to I') = \frac{5}{16\pi}\langle I020|I'0\rangle^2 Q_t^2, \qquad (2)$$

where $\langle I020|I'0\rangle$ is a Clebsch-Gordan coefficient and $I' = I - 2$.

In ^{184}Hg, the seven independent measurements of each of the lifetimes of the even-spin yrast states are presented in Fig. 6, as a function of the "ring" angle at which they were determined in Gammasphere.

It is worth noting that the new lifetime for the 4_1^+ state in ^{186}Hg is smaller than the previously measured value from Ref. [31]. The discrepancy in the first measurement is likely due to complications that the authors encountered in resolving the doublet and subsequent assumptions that were made.

TABLE I. Properties of the states investigated in this study. The uncertainties presented on τ_{av} represent the 1σ statistical error and include an additional systematic uncertainty which accounts for the choice of the fitting function and relativistic effects [27], typically $\leqslant 3\%$. γ-ray energies (E_γ) and branching fractions (b.f.) of the depopulating γ-ray transitions (corrected for internal conversion), as well as spin and parity (I^π) values, are taken from Refs. [20,21]. In cases where only one depopulating transition is observed, b.f. is assumed to be equal to unity. τ_{prev} values from Refs. [31–33] are shown for comparison.

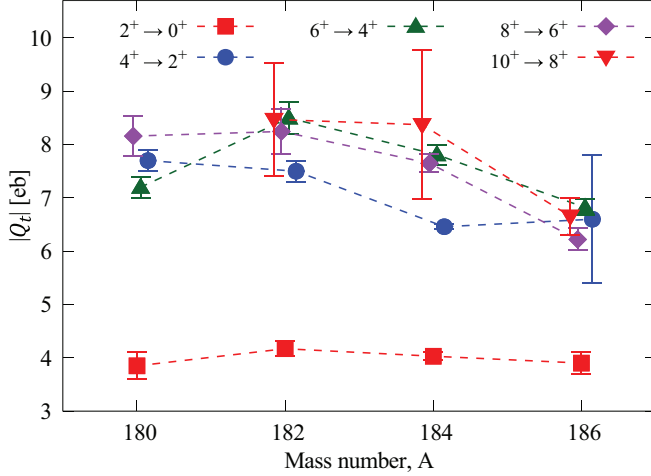|	I^π ($\hbar$)	E_γ (keV)	b.f.	τ_{av} (ps)	τ_{prev} (ps)	$B(E2)\downarrow$ (W.u.)	$|Q_t|$ (e b)
^{184}Hg	2_1^+	366.8	1	35.7(15)	30(7)	52(2)	4.04(8)
	4_1^+	287.0	0.959(4)	30.2(10)	32.8(34)	191(6)	6.46(11)
	6_1^+	340.1	1	8.7(4)	8.1(31)	308(15)	7.81(19)
	8_1^+	418.3	1	3.19(14)	$2.9^{+1.1}_{-1.6}$	309(13)	7.65(17)
	9_3	329.1	0.65(16)	12.1(8)		169(40)	5.6(7)
^{186}Hg	2_1^+	405.3	1	24(3)	26(4)	47(6)	3.9(2)
	4_1^+	402.7	0.93(2)	5.6(20)	13(4)	200(70)	6.6(12)
	6_1^+	356.8	1	9.1(4)	7(3)	231(10)	6.82(15)
	8_1^+	424.2	1	4.5(3)	≈ 4	202(14)	6.2(2)
	10_1^+	488.9	1	1.9(2)		238(25)	6.7(4)

FIG. 7. (Color online) Experimental $|Q_t|$ values, extracted from measured lifetimes, for yrast transitions in mercury nuclei as a function of mass number, A. Data for $A = 180, 182$ are taken from Ref. [18] and the $10^+ \rightarrow 8^+$ value for $A = 184$ is taken from Ref. [33]. Some markers are slightly offset from integer A values to maintain clarity.

IV. DISCUSSION

A. Yrast states in ^{184}Hg and ^{186}Hg

Transitional quadrupole moments, $|Q_t|$, for the even-spin yrast states are given in Fig. 7 for the mercury isotopes where $180 \leqslant A \leqslant 186$. The 2^+ states show no strong variation in $|Q_t|$ with mass number, whereas the collectivity of the 4^+ states reduces with increasing mass number. This can be compared to the energy level systematics in Fig. 1 where the energy of the intruder states reaches a minimum at $A = 182$.

B. The 9_3 state in ^{184}Hg

After the even-spin, positive-parity yrast band in ^{184}Hg, the most populated band is the odd-spin rotational band built upon the $I = 5$ state, observed at 1.848 MeV, which becomes yrast at around 4 MeV. Analogous bands have been observed in the neighboring isotopes, specifically ^{178}Hg [34] and ^{180}Hg [35] and their structure discussed in terms of octupole correlations. Lifetime measurements of states in this band in ^{182}Hg have been performed and a consistency in the structure of these states has been extended to ^{184}Hg using the energy displacement of states differing by $3\hbar$ [19]. The quadrupole moment measured here for the $9_3 \rightarrow 7_3$ transition in ^{184}Hg, $|Q_t| = 5.6(7) \, e$ b, is similar to that of the even-spin yrast band, $|Q_t| \simeq 7.7 \, e$ b, although it is smaller than those measured in the lighter isotopes.

C. Two-state mixing calculations

To shed light on the properties of the coexisting structures in these light mercury isotopes, phenomenological two-band mixing calculations were carried out using the assumption of a spin-independent interaction between two rotational structures. In the calculations, the variable moment of inertia (VMI) model [36] was used to fit known level energies of

TABLE II. Wave-function amplitudes of the normal configuration, α_I, at each spin, I, and spin-independent interaction strengths between members of the normal (n) band and intruder (i) band, $V = |\langle I_n | V_I | I_i \rangle|$ (equal for all values of I), calculated using the model described in the text. The extracted unperturbed bandhead energies are denoted by E_0^n and E_0^i for the normal and intruder bands, respectively.

Nucleus		I ($\hbar$)	$|\alpha_I|$
^{180}Hg	$V = 82.1$ keV	0	0.9799
		2	0.7722
	$E_0^n = 16.7$ keV	4	0.1571
		6	0.0817
	$E_0^i = 403.3$ keV	8	0.0546
		10	0.0408
^{182}Hg	$V = 89.4$ keV	0	0.9606
		2	0.5382
	$E_0^n = 25.9$ keV	4	0.1781
		6	0.1003
	$E_0^i = 309.0$ keV	8	0.0697
		10	0.0534
^{184}Hg	$V = 84.7$ keV	0	0.9725
		2	0.7172
	$E_0^n = 20.4$ keV	4	0.2014
		6	0.1025
	$E_0^i = 353.4$ keV	8	0.0679
		10	0.0506
^{186}Hg	$V = 66.3$ keV	0	0.9915
		2	0.9506
	$E_0^n = 8.9$ keV	4	0.2604
		6	0.0978
	$E_0^i = 505.4$ keV	8	0.0587
		10	0.0416
^{188}Hg	$V = 76.3$ keV	0	0.9954
		2	0.9884
	$E_0^n = 7.8$ keV	4	0.8933
		6	0.2467
	$E_0^i = 791.8$ keV	8	0.1095
		10	0.0691

rotational bands built upon the first two 0^+ states, up to and including $I^\pi = 10^+$ and 4^+ for yrast and nonyrast bands, respectively. Employing the method of Lane *et al.* [37], one can derive the wave-function amplitudes of the two configurations from the mixing strengths. These are shown in Table II along with the mixing strength, V, for each isotope and the bandhead energies of the two configurations.

Similar mixing calculations have previously been performed for ^{180,182,184}Hg [38]. The present results for ^{180,182}Hg differ due to the inclusion of nonyrast states identified in recent studies [8,10], which provide additional constraints on the calculations. The calculation for ^{184}Hg presented in Table II is essentially identical to that in Ref. [38]. It places the $I = 2$ member of the intruder band just 5 keV above the corresponding state in the normal band before mixing. This leads to almost complete mixing between the states, producing a first-excited 2^+ state which comprises 51% of the
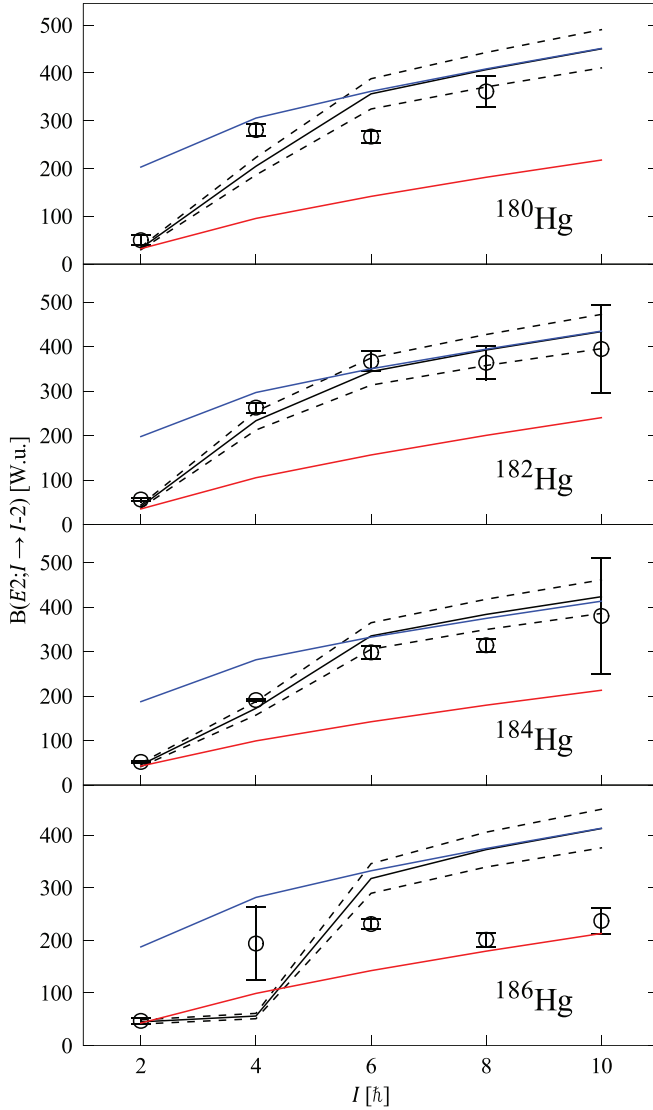
FIG. 8. (Color online) Experimental $B(E2)$ values measured in this work (points) plotted as a function of spin and compared to those extracted from the mixing calculations (solid black line; dashed line represents the uncertainty in the constant, k). For reference, the intraband $B(E2)$ values calculated for the pure unperturbed normal (red) and intruder (blue) bands are also shown. Data for ^{180,182}Hg are taken from Ref. [18] and the point at $I = 10\,\hbar$ in ^{184}Hg is taken from Ref. [33].

normal configuration and 49% of the intruder configuration. An alternative calculation in which the order of these states is reversed was also performed and yielded very similar parameters to those presented in Table II. In this scenario the unmixed states are nearly degenerate, so the degree of mixing is even greater. The resulting $B(E2)$ values (presented later in Fig. 8) are not significantly different, so in what follows only the results from the former calculation are discussed.

Low-lying levels in ^{184,186}Hg have also been interpreted assuming the mixing of spherical and deformed states [39], while an α-plus-rotor model has been used to extract spin-dependent interaction strengths and mixing amplitudes in ^{182,184,186}Hg [5]. The latter study predicted a contribution of

the more strongly deformed structure to the 2_1^+ state in ^{182}Hg of 76%, comparing very well to the value of 71% obtained in this work. We note here that this contribution drops to only 2.3% for the same state in ^{188}Hg. The corresponding isotones in the platinum nuclei were also interpreted recently using two-band mixing calculations, and qualitatively similar conclusions were drawn regarding a strong degree of mixing for the low-spin states [38,40].

It is possible to determine the transitional quadrupole moment of the unperturbed $I \rightarrow I - 2$ transitions in the normal (n) and intruder bands (i), Q_I, using an average of the moment of inertia of the two states, $\mathcal{J}_I'$, such that [36]

$$Q_I = k\sqrt{\mathcal{J}_I'} = k\sqrt{(\mathcal{J}_I + \mathcal{J}_{I-2})/2}, \qquad (3)$$

where $\mathcal{J}_I$ is the moment of inertia for a pure state with spin I, extracted from the fit. An evaluated value of the constant, fitted to data in the neutron-deficient $A = 170$ region, $k = 45(2)\,e$ b keV$^{-1/2}$ [41], was used in this study. Combining knowledge of the wave-function amplitudes with the intrinsic quadrupole moments of the pure states, Q_I, it is possible to extract the $B(E2; I \rightarrow I - 2)$ values of the mixed states [37]. The relative sign of the intrinsic quadrupole moments of the two configurations must be assumed to be positive or negative and was found to best reproduce the data when positive. This feature has been noted in previous calculations [37,42] and is at odds with what is expected from the rotational model when two bands with the same K quantum number have an opposite sign of deformation, i.e., an oblate and a prolate band.

The results of the calculations for the yrast sequences are compared in Fig. 8 with those extracted from the lifetimes measured in this work. Good agreement is found for the majority of yrast transitions, even for cases where the states are strongly mixed. The observed discrepancies for $I \geqslant 6$ in ^{186}Hg may indicate a breakdown of the simple two-band picture as other structures begin to influence the yrast states [43,44]. For the nuclei presented in Fig. 8, the experimental and calculated $B(E2; 2_1^+ \rightarrow 0_1^+)$ values are similar in each isotope, while the $B(E2; 4_1^+ \rightarrow 2_1^+)$ varies and, in each case, is not consistent with a transition within either of the pure bands. The low $B(E2; 2_1^+ \rightarrow 0_1^+)$ value is interpreted as being due to a transition between the weakly deformed oblate 0^+ ground state and a more strongly deformed prolate 2^+ state [18]. However, the admixture of the normal and intruder configurations for the 0^+ and 2^+ states is unique in each isotope and a similar $B(E2)$ value is not necessarily indicative of similar structures across the mass range.

In Fig. 9, calculated $B(E2)$ values are plotted as a function of the energy difference between the pure, unmixed 0^+ bandheads. The parameters used in the calculations are those of ^{184}Hg, but since they are not too dissimilar for all of the isotopes, the curves can be considered representative of the mercury isotopes around the neutron midshell. The four isotopes compared have ΔE_0 values in the range 250–550 keV, marked by the vertical lines in Fig. 9. One clearly observes that above 200 keV the $B(E2; 2_1^+ \rightarrow 0_1^+)$ values remain constant, even though the square of the mixing amplitude of the $I = 2$ states, α_2^2, drops from 0.80 at 200 keV down to 0.015 at 1 MeV. In contrast, the $B(E2; 4_1^+ \rightarrow 2_1^+)$ values vary significantly in
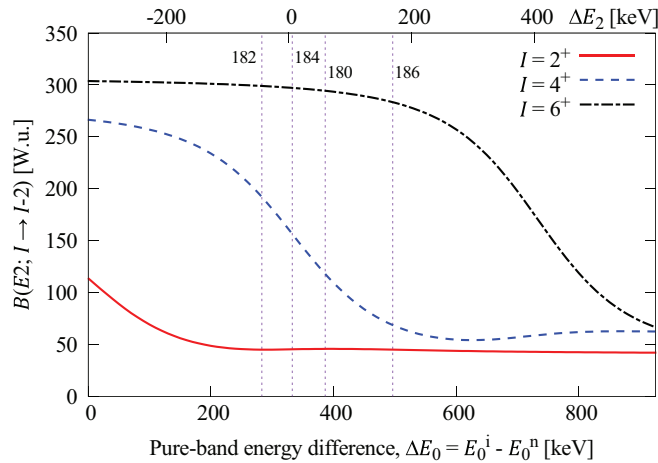
FIG. 9. (Color online) Representative $B(E2; I_1^+ \rightarrow (I-2)_1^+)$ values as a function of the energy separation of the pure bandheads, ΔE_0. The curves for $I = 2,4,6$ are calculated assuming the mixing strength and moments of inertia are equal to that extracted for ^{184}Hg. As a guide, the energy difference between the pure 2^+ states, ΔE_2, under this assumption is also shown. The dashed vertical lines show the extracted ΔE_0 values for each of the four isotopes.

the range of interest and are much more sensitive to α_2, while the $B(E2; 6_1^+ \rightarrow 4_1^+)$ values become more sensitive at larger bandhead energy differences.

V. SUMMARY AND CONCLUSIONS

Lifetimes of excited states have been measured by employing the RDDS technique. Yrast states up to $I^\pi = 8^+$ in ^{184}Hg and $I^\pi = 10^+$ in ^{186}Hg were studied. Distinct differences in deformation for the assigned normal and intruder bands could be shown. The lifetime of the 4_1^+ state in ^{186}Hg was found to be shorter than the previously measured value. Lifetimes of the 9_3 state in ^{184}Hg and the 10^+ state in ^{186}Hg were measured for the first time. The other lifetimes are consistent with previous measurements, while the uncertainty could be

reduced significantly. These more precise lifetime values, with those of Ref. [18], have been a vital input to the analysis of Coulomb excitation experiments at the REX-ISOLDE facility [45,46].

Rotational bands built upon the first two $I^\pi = 0^+$ states were considered in terms of a two-state mixing model and the mixing amplitudes of the two configurations extracted as a function of spin. It is observed that, while the ground state remains composed of predominantly one configuration, namely the assumed weakly deformed normal structure, in all of the even-mass mercury isotopes considered ($180 \leqslant A \leqslant 188$), the first excited 2^+ state changes dramatically in its composition. This is in contrast to a naïve interpretation emanating from the systematics of the 2^+ level energies and $B(E2; 2^+ \rightarrow 0^+)$ values, which are both strikingly similar across the mass range.

[1] J. Bonn, G. Huber, H.-J. Kluge, L. Kugler, and E. Otten, Phys. Lett. B **38**, 308 (1972).

[2] S. Frauendorf and V. Pashkkevich, Phys. Lett. B **55**, 365 (1975).

[3] G. Ulm *et al.*, Z. Phys. A **325**, 247 (1986).

[4] W. Nazarewicz, Phys. Lett. B **305**, 195 (1993).

[5] J. D. Richards, T. Berggren, C. R. Bingham, W. Nazarewicz, and J. Wauters, Phys. Rev. C **56**, 1389 (1997).

[6] R. Julin, K. Helariutta, and M. Muikku, J. Phys. G: Nucl. Part. Phys. **27**, R109 (2001).

[7] J. Tuli, Evaluated Nuclear Structure Data File (ENSDF), 2012.

[8] R. D. Page *et al.*, Phys. Rev. C **84**, 034308 (2011).

[9] M. Scheck *et al.*, Phys. Rev. C **83**, 037303 (2011).

[10] J. Elseviers *et al.*, Phys. Rev. C **84**, 034307 (2011).

[11] J. Kantele *et al.*, Z. Phys. A **289**, 157 (1979).

[12] K. Heyde and R. A. Meyer, Phys. Rev. C **37**, 2170 (1988).

[13] J. Wauters *et al.*, Phys. Rev. C **50**, 2768 (1994).

[14] J. Cole *et al.*, Phys. Rev. Lett. **37**, 1185 (1976).

[15] P. Joshi *et al.*, Int. J. Mod. Phys. E **3**, 757 (1994).

[16] K. Heyde and J. L. Wood, Rev. Mod. Phys. **83**, 1467 (2011).

[17] J. Wauters *et al.*, Z. Phys. A **345**, 21 (1993).

[18] T. Grahn *et al.*, Phys. Rev. C **80**, 014324 (2009).

[19] M. Scheck *et al.*, Phys. Rev. C **81**, 014310 (2010).

[20] J. Deng *et al.*, Phys. Rev. C **52**, 595 (1995).

[21] W. Ma *et al.*, Phys. Rev. C **47**, R5 (1993).

[22] I.-Y. Lee, Nuclear Phys. A **520**, c641 (1990).

[23] T. Lauritsen, GSSORT (unpublished).

[24] R. Brun and F. Rademakers, Nucl. Instrum. Methods Phys. Res., Sect. A **389**, 81 (1997).

[25] P. Petkov, Nucl. Instrum. Methods Phys. Res., Sect. A **349**, 289 (1994).

[26] G. Böhm, A. Dewald, P. Petkov, and P. von Brentano, Nucl. Instrum. Methods Phys. Res., Sect. A **329**, 248 (1993).

[27] A. Dewald, O. Möller, and P. Petkov, Prog. Part. Nucl. Phys. **67**, 786 (2012).

[28] B. Saha, NAPATAU or Tk-Lifetime-Analysis (unpublished).

[29] A. Dewald, S. Harissopulos, and P. Brentano, Z. Phys. A **334**, 163 (1989).

[30] P. Petkov, A. Dewald, and P. von Brentano, Nucl. Instrum. Methods Phys. Res., Sect. A **457**, 527 (2001).

[31] D. Proetel, R. M. Diamond, and F. S. Stephens, Phys. Lett. B **48**, 102 (1974).

[32] N. Rud, D. Ward, H. Andrews, R. Graham, and J. Geiger, Phys. Rev. Lett. **31**, 1421 (1973).

[33] W. C. Ma *et al.*, Phys. Lett. B **167**, 277 (1986).

[34] F. Kondev *et al.*, Phys. Rev. C **61**, 011303 (1999).

[35] F. Kondev *et al.*, Phys. Rev. C **62**, 044305 (2000).

[36] M. A. J. Mariscotti, G. Scharff-Goldhaber, and B. Buck, Phys. Rev. **178**, 1864 (1969).

[37] G. J. Lane *et al.*, Nuclear Phys. A **589**, 129 (1995).

[38] G. D. Dracoulis, Phys. Rev. C **49**, 3324 (1994).

[39] F. Dickmann and K. Dietrich, Z. Phys. **271**, 417 (1974).

[40] J. C. Walpe *et al.*, Phys. Rev. C **85**, 057302 (2012).

[41] G. D. Dracoulis *et al.*, Nucl. Phys. A **486**, 414 (1988).

[42] M. Guttormsen, Phys. Lett. B **105**, 99 (1981).

[43] H. Helppi, S. K. Saha, P. J. Daly, S. R. Faber, and T. L. Khoo, Phys. Rev. C **28**, 1382 (1983).

[44] J. Delaroche *et al.*, Phys. Rev. C **50**, 2332 (1994).

[45] A. Petts *et al.*, AIP Conf. Proc. **1090**, 414 (2009).

[46] N. Bree *et al.*, Phys. Rev. Lett. (to be published).